Generalised analytical framework for the stability studies of an AC microgrid

Manjunath Kallamadi, Vaskar Sarkar

Department of Electrical Engineering, Indian Institute of Technology Hyderabad, Hyderabad, India
E-mail: kmanjunath7@gmail.com

Published in *The Journal of Engineering*; Received on 9th March 2016; Accepted on 28th April 2016

Abstract: The objective is to address the small-signal stability analysis of a renewable-driven AC microgrid in the context of the practical usage and application. The state-space modelling of the system is generalised over all possible microgrid configurations. It is shown that there exist two simple templates to represent the dynamics of any type of load. The dynamics of any type of source (including the utility grid during the grid-connected operation) can be represented through a single template. Thus, the effective number of the different types of dynamic element is minimised and set fixed irrespective of the actual microgrid composition. In addition, similar loads are represented in the form of a single group to reduce computational complexity. A systematic procedure for constructing the system matrix using the prescribed source and load templates is discussed. The developed framework is applied on a test system having complex loads for both grid-connected and islanded operations. It is a common observation that system stability is influenced by the interactions between inertial and non-inertial components. To overcome this issue, suitable parameters are identified and tuned by performing system level study.

1 Introduction

A microgrid is basically the integration of small-scale distributed energy resources within a locality [1]. Being a low-inertia system, the dynamics of a microgrid needs to be carefully addressed so as to ensure a stable system operation. The stability studies of a microgrid differ from the stability studies of a conventional power grid in two respects. First of all, unlike conventional power systems, system level studies are often required for a microgrid with regard to the controller parameter tuning. The particular exercise requires the small-signal modelling of the entire microgrid system, followed by an eigenvalue analysis. Similar studies are performed in [2–5] for the droop coefficients tuning. The second major issue with regard to the stability analysis of a microgrid is the need for the incorporation of load (and transmission line) transients. In the case of conventional power systems, loads are typically represented by the ZIP (i.e. constant impedance, constant current and constant power) [6] model in the stability studies. The particular representation, in effect, employs the phasor approximation in which the load dynamics is substantially simplified by means of the time-scale decomposition. Similar load models are employed in [7] for the stability studies of a microgrid. However, the above mentioned time-scale decomposition may not be justified in the presence of low-inertia sources. It is, in fact, shown in [8] that the load dynamics can have significant effects on the stability of a microgrid. Therefore, the simplified load modelling approach may be inappropriate in the context of microgrid. The microgrid stability studies should be carried out with detailed representation of load transients. This, in turn, renders higher complexity in the stability analysis of a microgrid.

Though the stability study of a microgrid with the consideration of load dynamics is somewhat addressed in the literature, concentration is paid only on specific microgrid configurations. In [3–5, 9] only R and RL loads are considered. In [10–13], the microgrid stability studies are performed in the presence of only RL and induction motor loads. The microgrid configurations adopted in [14–16] have RL and voltage source rectifier (VSR) fed resistive loads. In addition, loads are placed either immediately after source capacitors [7, 16] or only at remote locations (i.e. away from source capacitor terminals) [4]. More importantly, in most of the cases, the stability analysis is carried out with only a few load elements. Owing to the limitation of referring to specific microgrid configurations with limited load elements, the works reported in the literature do not seem to provide a clear procedure for the small-signal modelling and stability studies of a practical microgrid.

The primary contribution of this paper is to develop a generalised algorithm for constructing the linearised state-space model of any arbitrary microgrid. The core of the proposed algorithm is built based on the findings that there can be two generalised templates for representing any load dynamics and one template for representing dynamics of any source. The template forms explored hide actual compositional complexity of a microgrid during the system state matrix construction. Therefore, there is no need to rework the whole procedure of system state matrix construction whenever there is a change in the microgrid configuration. This may, in turn, largely alleviate the stability studies of a microgrid.

In the present paper, both inertial (induction motor) and non-inertial (R, RL, thermostatic and VSR fed DC load) loads are considered. Additional delay block is used in source operating in drooping mode and phase locked loop (PLL) of VSR fed DC load to achieve better performance. This renders drooping mode source to work for both grid-connected and islanded modes of operation. Sometimes, PLL causes stability problems especially in low-inertia systems [17, 18]. Hence, in addition to droop parameters, time constants of the added delay blocks are also tuned in order to maintain system stability. Parameter tuning is performed such that stability is ensured in all the load changing scenarios.

The organisation of this paper is as follows. The templates for the generalised representation of load and source dynamics are derived in Section 2. The small-signal models of different components are shown in Section 3. The construction of the system matrix using proposed templates is explained in Section 4. In Section 5, a case study is performed to verify the generalised modelling. Finally, this paper is concluded in Section 6.

2 Generalised representation of load and source dynamics

The dynamic modelling of different elements is carried out in the d–q domain. A source or load element may have its own reference frame that governs its control dynamics. To describe the dynamics of the complete system, it is convenient to define a global reference frame. In steady state, the rotational speed of the global reference frame should converge to the rotational speed of a source or load reference frame so as to ensure the existence of an equilibrium. Therefore, the angle of the global reference frame is to be taken as the weighted sum of the local reference frame angles. The dynamic modelling

of each element is subsequently to be carried out over the global reference frame. For an available locally referred source or load dynamic model, it is, however, sufficient to convert only the terminal voltages and currents to the globally referred quantities. The *d*–*q* transformed quantities with respect to local and global reference frames are indicated by '*dq*' and '*DQ*', respectively, in superscripts or subscripts.

2.1 Load dynamics

It is possible to classify the load elements into a few categories by means of some simple qualitative analysis of general load attributes. Each load element is provided with only one network port for getting the power supply. Apart from the power circuit, a load element may also have its own control system. The power circuit and control system together define the complete load unit. Ideally, there should be only power supply input to the load unit. There are, however, a few instances in the literature in which all the VSR-based load units are fed with same frequency and angle signals from a common PLL [19]. That is, there are external signal inputs to the load control systems. However, in the case all the load control systems are to be implemented in global reference frame. Here, the use of PLL's can be avoided by directly communicating global frequency and angle signals.

The schematic arrangement of a VSR-based load unit considered in this paper is shown in Fig. 1*a*. The acronym VSC stands for voltage source converter. Fig. 2 shows the schematic diagram of a simple second-order PLL. It is to be noted that the coupling impedance and PLL are considered as a part of the VSR-based load unit.

With the above definition, loads are classified into two categories based on the terminal properties. For the first category, the current drawn by a load element does not indicate a state of the respective load element. The particular category is referred to as Class 1. Examples of such loads are the *R* loads and thermostatic loads. The modelling of thermostatic load is explained in [6]. There are certain other types of loads such as induction motor and VSR-based load for which the current drawn by a load element is a state variable (i.e. associated with an inductor). The respective load types fall in the second category, which is referred to as Class 2.

In principle, the dynamic modelling of an element should include only those quantities that are specifically related to the particular element or physical inputs. However, in order to refer the component in global reference, global frequency may also appear as input variable. The template of the load dynamics for Class 1 can be formulated as follows

$$p(x_{C1}) = f_{C1}\left(i_{C1}^{t,DQ},\ v_{C1}^{t,DQ},\ \omega_g,\ x_{C1},\ \lambda_{C1}\right) \tag{1}$$

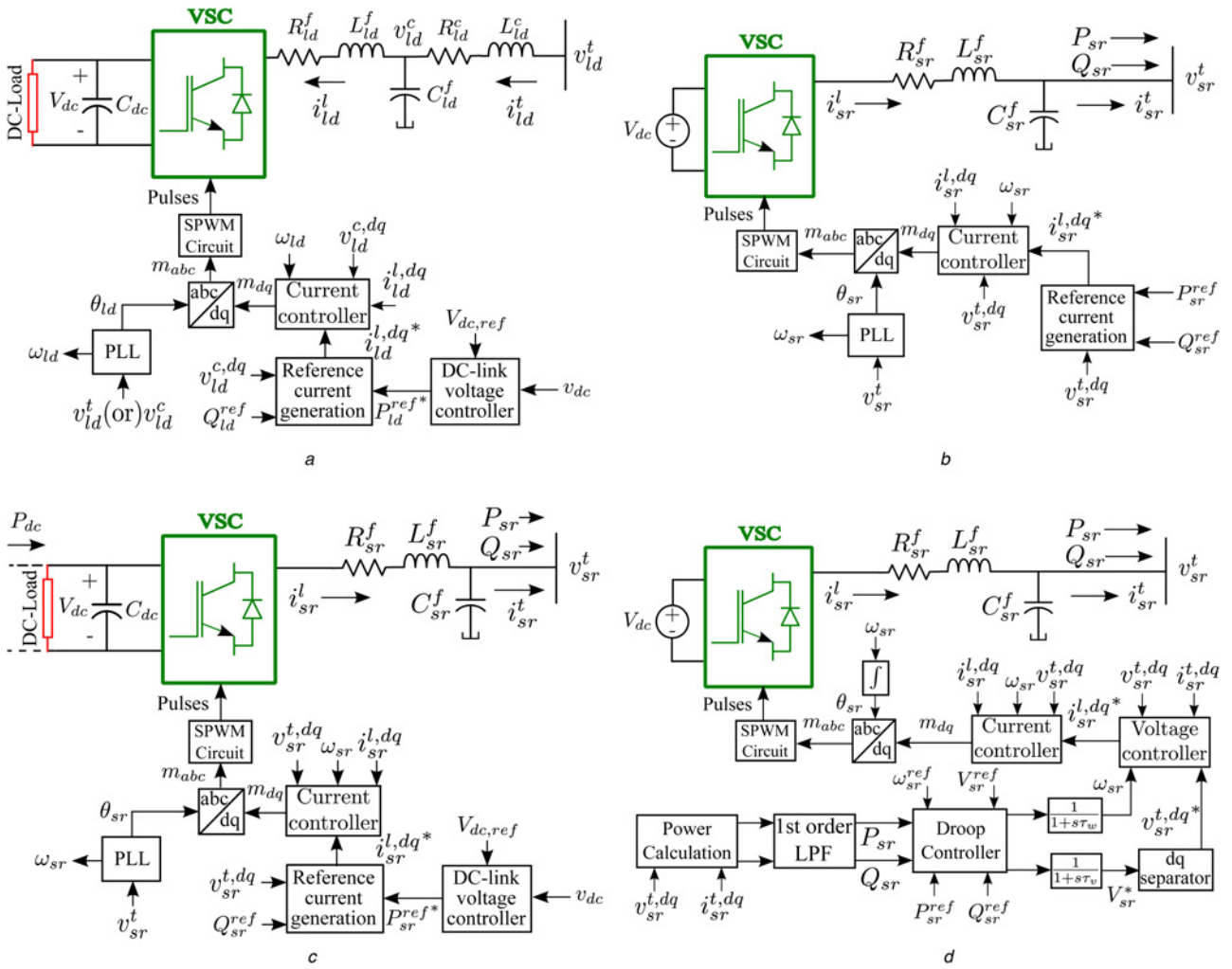

Fig. 1 *Block diagram representation of VSC operating as*
a VSR fed DC load
b Source in fixed power mode
c Source in fixed power mode with controlled DC voltage
d Source in drooping mode

J Eng 2016
doi: 10.1049/joe.2016.0045

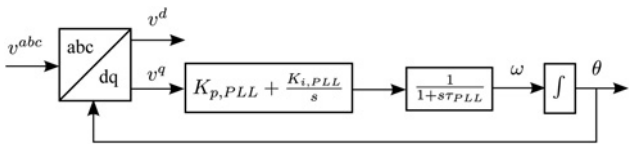

Fig. 2 *Schematic diagram of PLL*

$$g_{C1}\left(i_{C1}^{t,DQ},\ v_{C1}^{t,DQ},\ x_{C1},\ \lambda_{C1}\right) = 0. \tag{2}$$

Here, $\boldsymbol{x}_{C1}$ is the state variable vector associated with a Class 1 load element. The terminal voltage and current vectors (in DQ domain) are indicated by $v_{C1}^{t,DQ}$ and $i_{C1}^{t,DQ}$, respectively. The rotational speed of the global reference frame is indicated by ω_g. Variables $v_{C1}^{t,DQ}$ and ω_g are input quantities. Vector λ_{C1} contains fixed and operational load parameters. The differentiation operation is indicated by $p(\cdot)$. The current drawn by the load element is an algebraic variable, which is related to the state and input variables from (2). It is to be noted that there may be certain types of load with no state (R load). In that case, x_{C1} should be defined as a dummy state variable by equating (1) to zero. Defining a dummy state in the absence of any physical state alleviates the construction of the system matrix.

The template for the dynamics of a Class 2 load element appears as follows

$$p\left(x_{C2}\right) = f_{x,C2}\left(i_{C2}^{t,DQ},\ v_{C2}^{t,DQ},\ \omega_g,\ x_{C2},\ \lambda_{C2}\right) \tag{3}$$

$$p\left(i_{C2}^{t,DQ}\right) = f_{i,C2}\left(i_{C2}^{t,DQ},\ v_{C2}^{t,DQ},\ \omega_g,\ x_{C2},\ \lambda_{C2}\right). \tag{4}$$

Here, subscript 'C2' stands for Class 2. All the symbols used here have similar meanings as those in (1) and (2). However, the load current is now governed by a state equation rather than by an algebraic equation. As before, it may sometimes be required to define x_{C2} as a dummy state variable.

In spite of its small geographical span, a practical microgrid may have to serve power to many load elements. Individual modelling of load is usually employed because of the inapplicability of phasor approximation. This, in turn, largely increases the order of the system rendering computational complexity for stability analysis. One useful way to reduce the system order is to create groups of similar load elements. The concept of load grouping in the context of microgrid has already been employed in [13] for studying the effects of induction motors. The dynamics of a Class 1 load group thus formed can be formulated as follows

$$p\left(x_{C1}\right) = \hat{f}_{C1}\left(i_{\Sigma C1}^{t,DQ},\ v_{C1}^{t,DQ},\ \omega_g,\ x_{C1},\ \hat{\lambda}_{C1}\right) \tag{5}$$

$$\hat{g}_{C1}\left(i_{\Sigma C1}^{t,DQ},\ v_{C1}^{t,DQ},\ x_{C1},\ \hat{\lambda}_{C1}\right) = 0 \tag{6}$$

where

$$\hat{f}_{C1}\left(i_{\Sigma C1}^{t,DQ},\ v_{C1}^{t,DQ},\ \omega_g,\ x_{C1},\ \hat{\lambda}_{C1}\right) = f_{C1}\left(\frac{i_{\Sigma C1}^{t,DQ}}{n_{C1}},\ v_{C1}^{t,DQ},\ \omega_g,\ x_{C1},\ \hat{\lambda}_{C1}\right) \tag{7}$$

and

$$\hat{\lambda}_{C1} = \left[\lambda_{C1}^{T} \quad n_{C1}\right]^{T}. \tag{8}$$

Here, f_{C1} and λ_{C1} are obtained from an element that belongs to the particular load group. The number of individual elements within the load group and the net current drawn by the load group are indicated by n_{C1} and $i_{\Sigma C1}^{DQ}$, respectively. It is to be noted that the size of a load group serves only as a parameter in the load group dynamics. The order of the load group dynamics is independent of the load group size. The dynamics of a Class 2 load group can similarly be formulated as follows

$$p\left(x_{C2}\right) = \hat{f}_{x,C2}\left(i_{\Sigma C2}^{t,DQ},\ v_{C2}^{t,DQ},\ \omega_g,\ x_{C2},\ \hat{\lambda}_{C2}\right) \tag{9}$$

$$p\left(i_{\Sigma C2}^{t,DQ}\right) = \hat{f}_{i,C2}\left(i_{\Sigma C2}^{t,DQ},\ v_{C2}^{t,DQ},\ \omega_g,\ x_{C2},\ \hat{\lambda}_{C2}\right) \tag{10}$$

where

$$\hat{f}_{i,C2}\left(i_{\Sigma C2}^{t,DQ},\ v_{C2}^{t,DQ},\ \omega_g,\ x_{C2},\ \hat{\lambda}_{C2}\right) = n_{C2} f_{i,C2}\left(\frac{i_{\Sigma C2}^{t,DQ}}{n_{C2}},\ v_{C2}^{t,DQ},\ \omega_g,\ x_{C2},\ \lambda_{C2}\right). \tag{11}$$

Formation of load groups based on state coherency, in effect, replaces a set of similar load elements with an equivalent load of the same order as that of an original load element. As a consequence, the overall system order also comes down.

2.2 *Source dynamics*

There are basically three control modes for the source operation. Those are referred to as drooping mode, fixed power mode and the DC-link voltage controlling mode, respectively. The source configurations for different control modes are shown in Figs. 1*b*–*d*. Here, the acronym LPF stands for low-pass filter. Unlike a load element, the coupling impedance is not considered as a part of the source unit because there may be loads directly connected across the filter capacitor. The dynamics of any source can be represented through a unique template as follows:

$$p\left(\omega_{sr}\right) = f_{\omega,sr}\left(\omega_{sr},\ x_{sr},\ v_{sr}^{t,DQ},\ i_{sr}^{t,DQ},\ \omega_g\right) \tag{12}$$

$$p\left(x_{sr}\right) = f_{x,sr}\left(\omega_{sr},\ x_{sr},\ v_{sr}^{t,DQ},\ i_{sr}^{t,DQ},\ \omega_g\right) \tag{13}$$

$$p\left(v_{sr}^{t,DQ}\right) = f_{v,sr}\left(\omega_{sr},\ x_{sr},\ v_{sr}^{t,DQ},\ i_{sr}^{t,DQ},\ \omega_g\right). \tag{14}$$

Here, $v_{sr}^{t,DQ}$ is the voltage vector at the source terminal and ω_{sr} is the frequency of the source reference frame. Remaining states are represented by the vector x_{sr}. Vector $i_{sr}^{t,DQ}$ corresponds to the source terminal currents.

It is to be noted that the source configurations shown in Figs. 1*b*–*d* are only the representatives of different control modes. There can be additional controllers in the source control system. For example, Kahrobaeian and Mohamed [11] introduced additional compensators in the source modelling to minimise oscillations. However, this does not change the template of the source dynamics. Only, the $\boldsymbol{x}_{sr}$ vector needs to be modified in that case.

For the stability analysis of a grid-connected microgrid, the utility grid should be represented by a voltage source with constant magnitude, angle and frequency. The dynamics of the respective voltage source can also be expressed in the above form. The dynamics of a capacitor can be similarly described. However, for both the cases, ω_{sr} and x_{sr} will be dummy state variables.

3 Small-signal modelling of system components

In this section, the small-signal modelling of sources, lines and loads are discussed. It is required to organise the small-signal models in suitable forms to develop a systematic procedure for the construction of the system matrix. The required organisations of state and input matrices for each element are shown below.

doi: 10.1049/joe.2016.0045

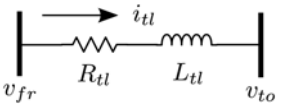

Fig. 3 *Physical representation of a line*

3.1 Source modelling

The small-signal model of a source is organised as follows

$$\begin{bmatrix} p(\Delta\omega_{\rm sr}) \\ p(\Delta x_{\rm sr}) \\ p(\Delta v_{\rm sr}^{\rm t,DQ}) \end{bmatrix} = \begin{bmatrix} A_{\omega\omega}^{\rm sr} & A_{\omega x}^{\rm sr} & A_{\omega v}^{\rm sr} \\ A_{x\omega}^{\rm sr} & A_{xx}^{\rm sr} & A_{xv}^{\rm sr} \\ A_{v\omega}^{\rm sr} & A_{vx}^{\rm sr} & A_{vv}^{\rm sr} \end{bmatrix} \begin{bmatrix} \Delta\omega_{\rm sr} \\ \Delta x_{\rm sr} \\ \Delta v_{\rm sr}^{\rm t,DQ} \end{bmatrix} + \begin{bmatrix} A_{\omega\omega_{\rm g}}^{\rm sr} & A_{\omega i}^{\rm sr} \\ A_{x\omega_{\rm g}}^{\rm sr} & A_{xi}^{\rm sr} \\ A_{v\omega_{\rm g}}^{\rm sr} & A_{vi}^{\rm sr} \end{bmatrix} \begin{bmatrix} \Delta\omega_{\rm g} \\ \Delta i_{\rm sr}^{\rm t,DQ} \end{bmatrix}. \quad (15)$$

Here, the state and input matrices are partitioned according to the variable groups that are formed in (12)–(14). Sub-matrices $A_{\omega\omega}^{\rm sr}$, $A_{\omega x}^{\rm sr}$, $A_{\omega v}^{\rm sr}$, $A_{\omega i}^{\rm sr}$, $A_{\omega\omega_{\rm g}}^{\rm sr}$, $A_{x\omega}^{\rm sr}$ and $A_{v\omega}^{\rm sr}$ should be set to zeros if $\omega_{\rm sr}$ is a dummy variable. Similar method is followed for other dummy variables.

3.2 Line modelling

The physical representation of a line is shown in Fig. 3. The small-signal state-space model of line dynamics appears as follows

$$p\left(\Delta i_{\rm tl}^{DQ}\right) = \left[A_{ii}^{\rm tl}\right]\left[\Delta i_{\rm tl}^{DQ}\right] + \begin{bmatrix} A_{i\omega_{\rm g}}^{\rm tl} & A_{iv_{\rm fr}}^{\rm tl} & A_{iv_{\rm to}}^{\rm tl} \end{bmatrix} \begin{bmatrix} \Delta\omega_{\rm g} \\ \Delta v_{\rm fr}^{DQ} \\ \Delta v_{\rm to}^{DQ} \end{bmatrix}. \quad (16)$$

3.3 Load modelling

The small-signal representation of the dynamics of a Class 1 load appears as follows

$$p(\Delta x_{\rm C1}) = \left[A_{xx}^{\rm C1}\right]\Delta x_{\rm C1} + \begin{bmatrix} A_{x\omega_{\rm g}}^{\rm C1} & A_{xv}^{\rm C1} \end{bmatrix} \begin{bmatrix} \Delta\omega_{\rm g} \\ \Delta v_{\rm C1}^{\rm t,DQ} \end{bmatrix} \quad (17)$$

$$\Delta i_{\rm C1}^{\rm t,DQ} = \left[A_{ix}^{\rm C1}\right]\Delta x_{\rm C1} + \begin{bmatrix} A_{i\omega_{\rm g}}^{\rm C1} & A_{iv}^{\rm C1} \end{bmatrix} \begin{bmatrix} \Delta\omega_{\rm g} \\ \Delta v_{\rm C1}^{\rm t,DQ} \end{bmatrix}. \quad (18)$$

Similarly, the dynamics of a Class 2 load can be represented in small-signal form as follows

$$p(\Delta x_{\rm C2}) = \begin{bmatrix} A_{xx}^{\rm C2} & A_{xi}^{\rm C2} \end{bmatrix} \begin{bmatrix} \Delta x_{\rm C2} \\ \Delta i_{\rm C2}^{\rm t,DQ} \end{bmatrix} + \begin{bmatrix} A_{x\omega_{\rm g}}^{\rm C2} & A_{xv}^{\rm C2} \end{bmatrix} \begin{bmatrix} \Delta\omega_{\rm g} \\ \Delta v_{\rm C2}^{\rm t,DQ} \end{bmatrix} \quad (19)$$

$$p\left(\Delta i_{\rm C2}^{\rm t,DQ}\right) = \begin{bmatrix} A_{ix}^{\rm C2} & A_{ii}^{\rm C2} \end{bmatrix} \begin{bmatrix} \Delta x_{\rm C2} \\ \Delta i_{\rm C2}^{\rm t,DQ} \end{bmatrix} + \begin{bmatrix} A_{i\omega_{\rm g}}^{\rm C2} & A_{iv}^{\rm C2} \end{bmatrix} \times \begin{bmatrix} \Delta\omega_{\rm g} \\ \Delta v_{\rm C2}^{\rm t,DQ} \end{bmatrix}. \quad (20)$$

4 System modelling

All the buses in the microgrid network are initially classified into two categories. The network buses at which sources are connected are referred to as source buses. Remaining buses are called as remote buses.

To build the small-signal state-space model of the system, all the algebraic variables associated with different components are to be expressed in terms of state variables. Algebraic variables include source terminal currents, remote bus voltages, line terminal voltages, Class 1 load currents and the rotational speed of the global reference frame. The remaining variables are state variables. The state variables of the system are organised as follows

$$\Delta\boldsymbol{X}_{\rm sys} = [\,\Delta\boldsymbol{\omega}_{\rm sr}^{\rm T} \;\; \Delta\boldsymbol{x}_{\rm sr}^{\rm T} \;\; \Delta\boldsymbol{i}_{\rm C2}^{\rm t,DQ^T} \;\; \Delta\boldsymbol{x}_{\rm C2}^{\rm T} \;\; \Delta\boldsymbol{x}_{\rm C1}^{\rm T} \;\; \Delta\boldsymbol{i}_{\rm tl}^{DQ^T} \;\; \Delta\boldsymbol{v}_{\rm sr}^{\rm t,DQ^T}\,]^{\rm T}. \quad (21)$$

The state variable vectors $\Delta\boldsymbol{\omega}_{\rm sr}$ and $\Delta\boldsymbol{x}_{\rm sr}$ are arranged as

$$\Delta\boldsymbol{\omega}_{\rm sr} = \left[\,\Delta\omega_{\rm sr}^{(1)} \;\; \Delta\omega_{\rm sr}^{(2)} \;\; \cdots \;\; \Delta\omega_{\rm sr}^{(N_{\rm sr})}\,\right]^{\rm T} \quad (22)$$

$$\Delta\boldsymbol{x}_{\rm sr} = \left[\,\Delta x_{\rm sr}^{(1)^{\rm T}} \;\; \Delta x_{\rm sr}^{(2)^{\rm T}} \;\; \cdots \;\; \Delta x_{\rm sr}^{(N_{\rm sr})^{\rm T}}\,\right]^{\rm T}. \quad (23)$$

Here, $N_{\rm sr}$ indicates the number of sources present in the system. The bracketed superscripts indicate source indices. The other state vectors $\Delta\boldsymbol{i}_{\rm C2}^{\rm t,DQ}$, $\Delta\boldsymbol{x}_{\rm C2}$, $\Delta\boldsymbol{x}_{\rm C1}$, $\Delta\boldsymbol{i}_{\rm tl}^{DQ}$ and $\Delta\boldsymbol{v}_{\rm sr}^{\rm t,DQ}$ are also arranged in the same manner.

The system state equations before the elimination of algebraic variables can be written as follows

$$p\left(\Delta\boldsymbol{X}_{\rm sys}\right) = \boldsymbol{A}_X^{\rm sys}\Delta\boldsymbol{X}_{\rm sys} + \boldsymbol{A}_{\omega_{\rm g}}^{\rm sys}\Delta\omega_{\rm g} + \boldsymbol{A}_{i_{\rm sr}}^{\rm sys}\Delta\boldsymbol{i}_{\rm sr}^{\rm t,DQ} + \boldsymbol{A}_{v_{\rm fr}}^{\rm sys}\Delta\boldsymbol{v}_{\rm fr}^{DQ} + \boldsymbol{A}_{v_{\rm to}}^{\rm sys}\Delta\boldsymbol{v}_{\rm to}^{DQ} + \boldsymbol{A}_{v_{\rm C1}}^{\rm sys}\Delta\boldsymbol{v}_{\rm C1}^{\rm t,DQ} + \boldsymbol{A}_{v_{\rm C2}}^{\rm sys}\Delta\boldsymbol{v}_{\rm C2}^{\rm t,DQ} \quad (24)$$

where

$$\boldsymbol{A}_X^{\rm sys} = \begin{bmatrix} \boldsymbol{A}_{\omega\omega}^{\rm sr} & \boldsymbol{A}_{\omega x}^{\rm sr} & \boldsymbol{0} & \boldsymbol{0} & \boldsymbol{0} & \boldsymbol{0} & \boldsymbol{A}_{\omega v}^{\rm sr} \\ \boldsymbol{A}_{x\omega}^{\rm sr} & \boldsymbol{A}_{xx}^{\rm sr} & \boldsymbol{0} & \boldsymbol{0} & \boldsymbol{0} & \boldsymbol{0} & \boldsymbol{A}_{xv}^{\rm sr} \\ \boldsymbol{0} & \boldsymbol{0} & \boldsymbol{A}_{ii}^{\rm C2} & \boldsymbol{A}_{ix}^{\rm C2} & \boldsymbol{0} & \boldsymbol{0} & \boldsymbol{0} \\ \boldsymbol{0} & \boldsymbol{0} & \boldsymbol{A}_{xi}^{\rm C2} & \boldsymbol{A}_{xx}^{\rm C2} & \boldsymbol{0} & \boldsymbol{0} & \boldsymbol{0} \\ \boldsymbol{0} & \boldsymbol{0} & \boldsymbol{0} & \boldsymbol{0} & \boldsymbol{A}_{xx}^{\rm C1} & \boldsymbol{0} & \boldsymbol{0} \\ \boldsymbol{0} & \boldsymbol{0} & \boldsymbol{0} & \boldsymbol{0} & \boldsymbol{0} & \boldsymbol{A}_{ii}^{\rm tl} & \boldsymbol{0} \\ \boldsymbol{A}_{v\omega}^{\rm sr} & \boldsymbol{A}_{vx}^{\rm sr} & \boldsymbol{0} & \boldsymbol{0} & \boldsymbol{0} & \boldsymbol{0} & \boldsymbol{A}_{vv}^{\rm sr} \end{bmatrix} \quad (25)$$

$$\boldsymbol{A}_{i_{\rm sr}}^{\rm sys} = \left[\,\boldsymbol{A}_{wi}^{\rm sr^T} \;\; \boldsymbol{A}_{xi}^{\rm sr^T} \;\; \boldsymbol{0} \;\; \boldsymbol{0} \;\; \boldsymbol{0} \;\; \boldsymbol{0} \;\; \boldsymbol{A}_{vi}^{\rm sr^T}\,\right]^{\rm T} \quad (26)$$

$$\boldsymbol{A}_{v_{\rm C1}}^{\rm sys} = \left[\,\boldsymbol{0} \;\; \boldsymbol{0} \;\; \boldsymbol{0} \;\; \boldsymbol{0} \;\; \boldsymbol{A}_{xv}^{\rm C1^T} \;\; \boldsymbol{0} \;\; \boldsymbol{0}\,\right]^{\rm T} \quad (27)$$

$$\boldsymbol{A}_{v_{\rm C2}}^{\rm sys} = \left[\,\boldsymbol{0} \;\; \boldsymbol{0} \;\; \boldsymbol{A}_{iv}^{\rm C2^T} \;\; \boldsymbol{A}_{xv}^{\rm C2^T} \;\; \boldsymbol{0} \;\; \boldsymbol{0} \;\; \boldsymbol{0}\,\right]^{\rm T} \quad (28)$$

$$\boldsymbol{A}_{v_{\rm fr}}^{\rm sys} = \left[\,\boldsymbol{0} \;\; \boldsymbol{0} \;\; \boldsymbol{0} \;\; \boldsymbol{0} \;\; \boldsymbol{0} \;\; \boldsymbol{A}_{iv_{\rm fr}}^{\rm tl\;T} \;\; \boldsymbol{0}\,\right]^{\rm T} \quad (29)$$

$$\boldsymbol{A}_{v_{\rm to}}^{\rm sys} = \left[\,\boldsymbol{0} \;\; \boldsymbol{0} \;\; \boldsymbol{0} \;\; \boldsymbol{0} \;\; \boldsymbol{0} \;\; \boldsymbol{A}_{iv_{\rm to}}^{\rm tl\;T} \;\; \boldsymbol{0}\,\right]^{\rm T} \quad (30)$$

$$\boldsymbol{A}_{\omega_{\rm g}}^{\rm sys} = \left[\,\boldsymbol{A}_{\omega\omega_{\rm g}}^{\rm sr\,T} \;\; \boldsymbol{A}_{x\omega_{\rm g}}^{\rm srT} \;\; \boldsymbol{A}_{i\omega_{\rm g}}^{\rm C2\;T} \;\; \boldsymbol{A}_{x\omega_{\rm g}}^{\rm C2\;T} \;\; \boldsymbol{A}_{x\omega_{\rm g}}^{\rm C1\;T} \;\; \boldsymbol{A}_{i\omega_{\rm g}}^{\rm tl\;T} \;\; \boldsymbol{A}_{v\omega_{\rm g}}^{\rm sr\,T}\,\right]^{\rm T}. \quad (31)$$

All the sub-matrices on the right-hand sides of (25)–(30) should be organised in block diagonal form. For example, $\boldsymbol{A}_{\omega\omega}^{\rm sr}$ is organised as follows

$$\boldsymbol{A}_{\omega\omega}^{\rm sr} = {\rm diag}\left(A_{\omega\omega}^{\rm sr(1)},\, A_{\omega\omega}^{\rm sr(2)},\, \ldots,\, A_{\omega\omega}^{\rm sr(N_{\rm sr})}\right). \quad (32)$$

On the other hand, the sub-matrices in (31) take the following form

$$\boldsymbol{A}_{\omega\omega_{\rm g}}^{\rm sr} = \left[\,A_{\omega\omega_{\rm g}}^{\rm sr(1)} \;\; A_{\omega\omega_{\rm g}}^{\rm sr(2)} \;\; \ldots \;\; A_{\omega\omega_{\rm g}}^{\rm sr(N_{\rm sr})}\,\right]^{\rm T}. \quad (33)$$

J Eng 2016
doi: 10.1049/joe.2016.0045

The dimensions of all the zero matrix blocks in (25)–(30) are consistent with the dimensions of the respective state variable blocks as per the arrangement in (21).

Voltage and current algebraic variables can be expressed in terms of state variables by means of incidence matrices. Separate incidence matrices are to be defined for source and remote buses. Each incidence matrix is basically a block matrix with entries being (2×2) identity or zero sub-matrices based on incidence of a particular element at a bus. Rows and columns of an incidence matrix correspond to buses and elements, respectively. All the incidence matrices are represented by the symbol $M_{(.)}^{(.)}$. The incidence matrices corresponding to source and remote buses are indicated by 'sb' and 'rb', respectively, in superscripts. The bus incidences of 'from' and 'to' terminals of transmission lines are separately shown with subscripts 'tlf' and 'tlt', respectively.

The line and load terminal voltages are expressed in terms of bus voltages by modifying (24) as follows

$$p\left(\Delta \boldsymbol{X}_{\text{sys}}\right) = \boldsymbol{A}_{X}^{\text{sys}} \Delta \boldsymbol{X}_{\text{sys}} + \boldsymbol{A}_{\omega_{\text{g}}}^{\text{sys}} \Delta \omega_{\text{g}} + \boldsymbol{A}_{i_{\text{sr}}}^{\text{sys}} \Delta \boldsymbol{i}_{\text{sr}}^{\text{t},DQ} + \boldsymbol{A}_{v_{\text{sb}}}^{\text{sys}} \Delta \boldsymbol{v}_{\text{sb}}^{DQ} + \boldsymbol{A}_{v_{\text{rb}}}^{\text{sys}} \Delta \boldsymbol{v}_{\text{rb}}^{DQ} \tag{34}$$

where

$$\boldsymbol{A}_{v_{\text{sb}}}^{\text{sys}} = \boldsymbol{A}_{v_{\text{C1}}}^{\text{sys}} \boldsymbol{M}_{C1}^{\text{sb}^{\text{T}}} + \boldsymbol{A}_{v_{\text{C2}}}^{\text{sys}} \boldsymbol{M}_{\text{C2}}^{\text{sb}^{\text{T}}} + \boldsymbol{A}_{v_{\text{fr}}}^{\text{sys}} \boldsymbol{M}_{\text{tl}}^{\text{sb}^{\text{T}}} \tag{35}$$

$$\boldsymbol{A}_{v_{\text{rb}}}^{\text{sys}} = \boldsymbol{A}_{v_{\text{C1}}}^{\text{sys}} \boldsymbol{M}_{\text{C1}}^{\text{rb}^{\text{T}}} + \boldsymbol{A}_{v_{\text{C2}}}^{\text{sys}} \boldsymbol{M}_{\text{C2}}^{\text{rb}^{\text{T}}} + \boldsymbol{A}_{v_{\text{fr}}}^{\text{sys}} \boldsymbol{M}_{\text{tl}}^{\text{rb}^{\text{T}}} \tag{36}$$

$$\boldsymbol{M}_{\text{tl}}^{\text{rb}} = \boldsymbol{M}_{\text{tlf}}^{\text{rb}} - \boldsymbol{M}_{\text{tlt}}^{\text{rb}} \tag{37}$$

$$\boldsymbol{M}_{\text{tl}}^{\text{sb}} = \boldsymbol{M}_{\text{tlf}}^{\text{sb}} - \boldsymbol{M}_{\text{tlt}}^{\text{sb}}. \tag{38}$$

Here, the source and remote bus voltage vectors are represented by $\boldsymbol{v}_{\text{sb}}^{DQ}$ and $\boldsymbol{v}_{\text{rb}}^{DQ}$, respectively.

The frequency of the global reference frame is taken as the weighted sum of source frequencies. That is

$$\Delta \omega_{\text{g}} = \boldsymbol{w}^{\text{T}} \Delta \omega_{\text{sr}}. \tag{39}$$

Here, $\boldsymbol{w}$ is an $(N_{\text{sr}} \times 1)$ vector containing the weight factors. The source bus voltages can directly be expressed in terms of source terminal voltages as follows

$$\Delta \boldsymbol{v}_{\text{sb}}^{DQ} = \boldsymbol{M}_{\text{sr}}^{\text{sb}^{\text{T}}} \Delta \boldsymbol{v}_{\text{sr}}^{\text{t},DQ}. \tag{40}$$

According to Kirchhoff's current law (KCL) at remote buses

$$\boldsymbol{M}_{\text{C1}}^{\text{rb}} \Delta \boldsymbol{i}_{\text{C1}}^{\text{t},DQ} + \boldsymbol{M}_{\text{C2}}^{\text{rb}} \Delta \boldsymbol{i}_{\text{C2}}^{\text{t},DQ} + \boldsymbol{M}_{\text{tl}}^{\text{rb}} \Delta \boldsymbol{i}_{\text{tl}}^{DQ} = \boldsymbol{0}. \tag{41}$$

From (18), the currents drawn by all the Class 1 load elements are expressed as follows

$$\Delta \boldsymbol{i}_{\text{C1}}^{\text{t},DQ} = \boldsymbol{A}_{iv}^{\text{C1}} \left(\boldsymbol{M}_{\text{C1}}^{\text{rb}^{\text{T}}} \Delta \boldsymbol{v}_{\text{rb}}^{DQ} + \boldsymbol{M}_{\text{C1}}^{\text{sb}^{\text{T}}} \Delta \boldsymbol{v}_{\text{sb}}^{DQ} \right) + \boldsymbol{A}_{ix}^{\text{C1}} \Delta \boldsymbol{x}_{\text{C1}} + \boldsymbol{A}_{i\omega_{\text{g}}}^{\text{C1}} \Delta \omega_{\text{g}}. \tag{42}$$

Here, the organisation of $\boldsymbol{A}_{iv}^{\text{C1}}$ and $\boldsymbol{A}_{ix}^{\text{C1}}$ is similar to that in (32). Matrices $\boldsymbol{A}_{i\omega_{\text{g}}}^{\text{C1}}$ and $\boldsymbol{A}_{\omega\omega_{\text{g}}}^{\text{sr}}$ have the similar organisation [as in (33)]. By substituting (42) into (41), the expression of the remote bus voltage vector in terms of state variables is shown below

$$\Delta \boldsymbol{v}_{\text{rb}}^{DQ} = \boldsymbol{\Gamma}_{v_{\text{rb}}} \Delta \boldsymbol{X}_{\text{sys}} \tag{43}$$

where

$$\boldsymbol{\Gamma}_{v_{\text{rb}}} = \boldsymbol{G} \left[\boldsymbol{M}_{\text{C1}}^{\text{rb}} \boldsymbol{A}_{i\omega_{\text{g}}}^{\text{C1}} \boldsymbol{w}^{\text{T}} \;\; \boldsymbol{0} \;\; \boldsymbol{M}_{\text{C2}}^{\text{rb}} \;\; \boldsymbol{0} \;\; \boldsymbol{M}_{\text{C1}}^{\text{rb}} \boldsymbol{A}_{ix}^{\text{C1}} \;\; \boldsymbol{M}_{\text{tl}}^{\text{rb}} \;\; \boldsymbol{M}_{\text{C1}}^{\text{rb}} \boldsymbol{A}_{iv}^{\text{C1}} \boldsymbol{M}_{\text{C1}}^{\text{sb}^{\text{T}}} \boldsymbol{M}_{\text{sr}}^{\text{sb}} \right]$$
$$\boldsymbol{G} = -\left(\boldsymbol{M}_{\text{C1}}^{\text{rb}} \boldsymbol{A}_{iv}^{\text{C1}} \boldsymbol{M}_{\text{C1}}^{\text{rb}^{\text{T}}} \right)^{-1}. \tag{44}$$

Similarly, the relationship between the source current vector and state variables can be established by writing KCL equations at source buses

$$\boldsymbol{M}_{\text{sr}}^{\text{sb}} \Delta \boldsymbol{i}_{\text{sr}}^{\text{t},DQ} = \boldsymbol{M}_{\text{C2}}^{\text{sb}} \Delta \boldsymbol{i}_{\text{C2}}^{\text{t},DQ} + \boldsymbol{M}_{\text{C1}}^{\text{sb}} \Delta \boldsymbol{i}_{\text{C1}}^{\text{t},DQ} + \boldsymbol{M}_{\text{tl}}^{\text{sb}} \Delta \boldsymbol{i}_{\text{tl}}^{DQ}. \tag{45}$$

From (42) and (45), the following relationship can be obtained

$$\boldsymbol{i}_{\text{sr}}^{\text{t},DQ} = \boldsymbol{\Gamma}_{i_{\text{sr}}} \Delta \boldsymbol{X}_{\text{sys}} \tag{46}$$

where (see equation at bottom of the page)

Relationships (39) and (40) can subsequently be written as follows:

$$\Delta \omega_{\text{g}} = \boldsymbol{\Gamma}_{\omega_{\text{g}}} \Delta \boldsymbol{X}_{\text{sys}} \tag{47}$$

$$\Delta \boldsymbol{v}_{\text{sb}}^{DQ} = \boldsymbol{\Gamma}_{v_{\text{sb}}} \Delta \boldsymbol{X}_{\text{sys}} \tag{48}$$

where

$$\boldsymbol{\Gamma}_{\omega_{\text{g}}} = \left[\boldsymbol{w}^{\text{T}} \;\; \boldsymbol{0} \;\; \boldsymbol{0} \;\; \boldsymbol{0} \;\; \boldsymbol{0} \;\; \boldsymbol{0} \;\; \boldsymbol{0} \right] \tag{49}$$

$$\boldsymbol{\Gamma}_{v_{\text{sb}}} = \left[\boldsymbol{0} \;\; \boldsymbol{0} \;\; \boldsymbol{0} \;\; \boldsymbol{0} \;\; \boldsymbol{0} \;\; \boldsymbol{0} \;\; \boldsymbol{M}_{\text{sr}}^{\text{sb}^{\text{T}}} \right]. \tag{50}$$

The final system state matrix after replacing (43), (46), (47) and (48) into (34), is shown below

$$\boldsymbol{A}_{\text{sys}} = \boldsymbol{A}_{X}^{\text{sys}} + \boldsymbol{A}_{\omega_{\text{g}}}^{\text{sys}} \boldsymbol{\Gamma}_{\omega_{\text{g}}x} + \boldsymbol{A}_{i_{\text{sr}}}^{\text{sys}} \boldsymbol{\Gamma}_{i_{\text{sr}}} + \boldsymbol{A}_{v_{\text{sb}}}^{\text{sys}} \boldsymbol{\Gamma}_{v_{\text{sb}}} + \boldsymbol{A}_{v_{\text{rb}}}^{\text{sys}} \boldsymbol{\Gamma}_{v_{\text{rb}}}. \tag{51}$$

The existence of dummy state variables in the state equations, however, increases the size of the system with unnecessary zero eigenvalues. The respective dummy states are removed by eliminating the corresponding rows and columns of the formulated system matrix. Moreover, there can be certain source frequency variables for which the time constants (i.e. τ_w as in Fig. 1*d*) are zero. Though the respective frequency variables can still be represented as states by means of variable transformation, the same may lead to procedural complexity. Alternatively, the system matrix can, first, be constructed by assigning non-zero time constants to the corresponding first-order delay blocks. It is to be noted that the time constant of a first-order delay block does not affect the system equilibrium. Subsequently, the elements corresponding to the above frequency variables in the state differentiation vector can be set to zero, from which the respective frequency variables can be replaced in terms of state variables in the other state equations.

5 Case study

A case study is performed for evaluating the ability of a microgrid to withstand load transitions under a complex loading condition. As mentioned previously, the system operation can be divided over

$$\boldsymbol{\Gamma}_{i_{\text{sr}}} = \boldsymbol{M}_{\text{sr}}^{\text{sb}^{-1}} \left[\boldsymbol{M}_{\text{C1}}^{\text{sb}} \boldsymbol{A}_{i\omega_{\text{g}}}^{\text{C1}} \boldsymbol{w}^{\text{T}} \;\; \boldsymbol{0} \;\; \boldsymbol{M}_{\text{C2}}^{\text{sb}} \;\; \boldsymbol{0} \;\; \boldsymbol{M}_{\text{C1}}^{\text{sb}} \boldsymbol{A}_{ix}^{\text{C1}} \;\; \boldsymbol{M}_{\text{tl}}^{\text{sb}} \;\; \boldsymbol{M}_{\text{C1}}^{\text{sb}} \boldsymbol{A}_{iv}^{\text{C1}} \boldsymbol{M}_{\text{C1}}^{\text{sb}^{\text{T}}} \boldsymbol{M}_{\text{sr}}^{\text{sb}} \right].$$

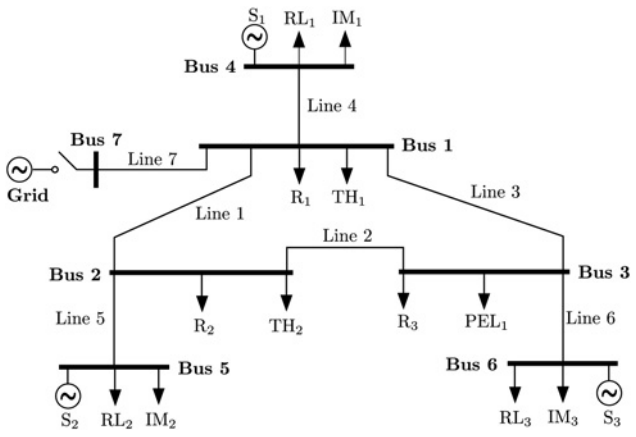

Fig. 4 *Test system*

certain time intervals. During a particular time interval, the system load profile remains almost constant. However, there may be significant load change whenever the system operation shifts from one time interval to the next time interval. The load transition takes place in the form of new load additions or drop-outs of some present loads. Following a load transition, the system should be able to quickly settle down to the new equilibrium. This, in turn, requires appropriate controller parameter tuning, which is demonstrated in this section.

The test system considered in this case study is shown in Fig. 4. The nominal bus voltage and system frequency are 400 V (line-to-line) and 50 Hz, respectively. The source and line details are provided in Tables 1 and 2, respectively. The feed-forward gains of all the current controllers are taken to be zero. All the sources are running in the drooping mode. The system load profile is shown below:

(i) Three sets (i.e. IM_1, IM_2 and IM_3) of $3-\phi$ induction motors.

Table 1 Source data

Source id.	Parameter	Value
S_1, S_3	active power rating	20 kW
	reactive power rating (minimum, maximum)	(16.46, 26.71) kVAr
	filter resistance	0.295 Ω
	filter inductance	1.47441 mH
	filter capacitance	429.5 μF
	proportional gain of voltage controller	0.2 Ω^{-1}
	integral gain of voltage controller	9.68 $\Omega^{-1}s^{-1}$
	proportional gain of current controller	1.47441 Ω
	integral gain of current controller	295.8 Ω/s
	cut-off frequency of LPF	31.41 rad/s
	time constant of voltage delay block	1×10^{-3} s
S_2	active power rating	10 kW
	reactive power rating (minimum, maximum)	(−0.049, 5.07) kVAr
	filter resistance	0.1 Ω
	filter inductance	1.35 mH
	filter capacitance	50 μF
	proportional gain of voltage controller	0.05 Ω^{-1}
	integral gain of voltage controller	390 $\Omega^{-1}s^{-1}$
	proportional gain of current controller	10.5 Ω
	integral gain of current controller	16,000 Ω/s
	cut-off frequency of LPF	31.41 rad/s
	time constant of voltage delay block	1×10^{-3} s

Table 2 Line data

Line id.	Resistance, Ω	Inductance, H
line 1	0.234	0.0005
line 2	0.215	0.0008
line 3	0.328	0.0005
line 4	0.1	0.000636
line 5	0.1	0.000636
line 6	0.1	0.000636
line 7	0.1	0.0003

(ii) One set (i.e. PEL_1) of VSR fed resistive loads.
(iii) Two sets (i.e. TH_1 and TH_2) of thermostatic loads.
(iv) Three sets (i.e. RL_1, RL_2 and RL_3) of RL loads.
(v) Three sets (i.e. R_1, R_2 and R_3) of normal R loads.

Each load set consists of similar load elements. The load parameter details are provided in Table 3.

All the controller parameters presented in Tables 1 and 3 are locally tuned by following the procedures explained in [20]. To tune PLL parameters, the time constant of the frequency delay block is initially taken as 1 ms. The following source controller parameters are to be tuned by carrying out a system level stability study:

- Active power droop coefficient.
- Reactive power droop coefficient.
- Voltage controller feed-forward gain.
- Time constant of the frequency delay block.

The value of each of the above parameters is taken to be the same for all the sources. The droop coefficients are expressed in per unit through the following relationships

$$d_p(\text{pu}) = d_{p_{\text{act}}}\left(\frac{P_{\max}}{\omega_n}\right) \tag{52}$$

$$d_q(\text{pu}) = d_{q_{\text{act}}}\left(\frac{Q_{\max}-Q_{\min}}{V_n}\right). \tag{53}$$

Here, d_p and d_q indicate the active power droop coefficient and the reactive power droop coefficient, respectively. Subscript 'act' indicates the actual unit, whereas 'pu' stands for per unit. The maximum active and reactive power generation capabilities of a source are indicated by $P_{\max}$ and $Q_{\max}$, respectively. Symbol $Q_{\min}$ represents the minimum reactive power generation capability. The nominal system frequency and bus voltage magnitude are indicated by ω_n and V_n, respectively. Apart from source parameters, the time constant of the PLL frequency delay block for a VSR load is also to be tuned through the system level study. However, the time constants of all the PLL frequency delay blocks are kept equal.

Table 4 shows the base case load profile as well as the load transition that takes place. The addition of new load elements may happen in the following sequence. First of all, certain load elements such as induction motors and VSR loads need to go through some start-up procedures. After being started up, the respective load elements remain in idling (i.e. no load) mode for certain time duration. Subsequently, those load elements are set to draw the desired amounts of power and the other load elements (i.e. the load elements that do not require special start-up procedure) are added. The corresponding time durations can be referred to as start-up, idling and pick-up periods.

As mentioned previously, there may be a special procedure for starting up a load element. However, the issue of starting up a

J Eng 2016
doi: 10.1049/joe.2016.0045

Table 3 Load data

Load id.	Parameter	Value
R_1, R_2, R_3	resistance	100 Ω, 70 Ω 50 Ω
RL_1	resistance	400 Ω
	inductance	0.6 H
RL_2	resistance	300 Ω
	inductance	0.5 H
RL_3	resistance	500 Ω
	inductance	0.4 H
IM_1, IM_2, IM_3	stator resistance	1.405 Ω
	stator inductance	0.005839 H
	mutual inductance	0.1722 H
	rotor resistance referred to stator side	1.395 Ω
	rotor inductance referred to stator side	0.005839 H
	number of poles	4
	moment of inertia	0.0131 kg m^2
	load torque (IM_1)	4.59169 Nm
	load torque (IM_2)	2.29584 Nm
	load torque (IM_3)	5.510028 Nm
PEL_1	coupling resistance	0.1 Ω
	coupling inductance	0.0001 H
	filter resistance	0.295
	filter inductance	1.47441 mH
	filter capacitance	429.5 μF
	DC-link voltage	900 V
	proportional gain of DC-link controller	3.095
	integral gain of DC-link controller	29.962
	proportional gain of current controller	1.47441 Ω
	integral gain of current controller	295.8 Ω/s
	DC capacitance	0.01 F
	DC conductance	2.469 $m\Omega^{-1}$
	proportional gain of PLL	1.5476
	integral gain of PLL	14.9814
TH_1, TH_2	proportional gain of proportional–integral (PI) controller	−0.00074
	integral gain of PI controller	−2.507
	time constant of thermostatic load	1×10^{-3} s
	gain of thermostatic load	−0.004
	reference temperature (TH_1)	300° K
	reference temperature (TH_2)	295° K
	ambient temperature (TH_1)	305° K
	ambient temperature (TH_2)	305° K

load element is ignored in this paper. It is rather assumed that an induction motor or VSR load can be started by following some appropriate procedure without affecting the system stability. The controller parameter tuning is carried out in a way so that the small-signal stability is maintained both at the equilibriums of

Table 4 Description of base case load profile and load transition

Load set	Number of elements		
	Base case	New addition	Drop-out
RL_1	5	0	0
RL_2	5	0	0
RL_3	5	3	0
TH_1	2	1	0
TH_2	2	0	0
PEL_1	2	1	0
IM_1	2	0	0
IM_2	2	0	0
IM_3	2	1	0

Table 5 Reference settings of sources

Id.	Case	Active power, W	Reactive power, VAr	Voltage, V
S_1	base case	13,375	−3097	397.6833
	load addition	15,476	−4555	397.4475
S_2	base case	5045	13,965	404.0703
	load addition	6067	13,157	403.9254
S_3	base case	10,054	8853	403.0378
	load addition	12,119	14,311	404.2717

idling and pick-up periods of the next time interval as well as at the equilibrium of the present time interval (i.e. base case). The reference set points of sources are changed only at the inception of the pick-up period.

Results are obtained for both the grid-connected and islanded operations. However, during the grid-connected operation, the utility grid is kept just in the stand-by mode. That is, no power exchange takes place between the utility grid and the microgrid in steady state. The assumption of zero power exchange at the base case equilibrium is made only for the sake of simplicity in simulation. The source reference set points are determined accordingly by means of load flow analysis. The power and voltage reference settings of sources corresponding to the base case and after the new load additions are shown in Table 5. The frequency reference is taken as 50 Hz.

The parameter tuning is carried out by means of particle swarm optimisation (PSO) [9] minimising the largest real part among all the non-zero eigenvalues of the linearised system matrix. The upper and lower limits kept on each parameter in the PSO technique are presented in Table 6. Symbol F indicates voltage controller feed-forward gain.

Results obtained from the PSO method are shown in Table 7. The same set of results is obtained with and without load grouping. It is revealed from the results in Table 7 that the time constant of the PLL frequency delay block is to be set much higher than the time constant of the source frequency delay block in the case of islanded operation. For the grid-connected operation, both the time constants need to be set at low values. In contrast, droop coefficients should be assigned higher values for grid-connected operation. The eigenvalues near imaginary axis for islanded and grid-connected operations are shown in Figs. 5*a* and *b*, respectively.

Table 6 Minimum and maximum limits considered for optimisation

Parameter	Minimum limit	Maximum limit
d_p, pu	1×10^{-5}	0.01
d_q, pu	1×10^{-5}	0.02
F	0	1
τ_w, s	0.0005	0.01
τ_{PLL}, s	0.0005	0.01

Table 7 System parameter settings

Parameter	Grid-connected mode	Stand-alone mode
d_p, pu	1.689×10^{-3}	1×10^{-5}
d_q, pu	0.0049	2.67×10^{-4}
F	0.832	0.814
τ_w, s	5.662×10^{-4}	0.0005
τ_{PLL}, s	6.226×10^{-4}	0.0028

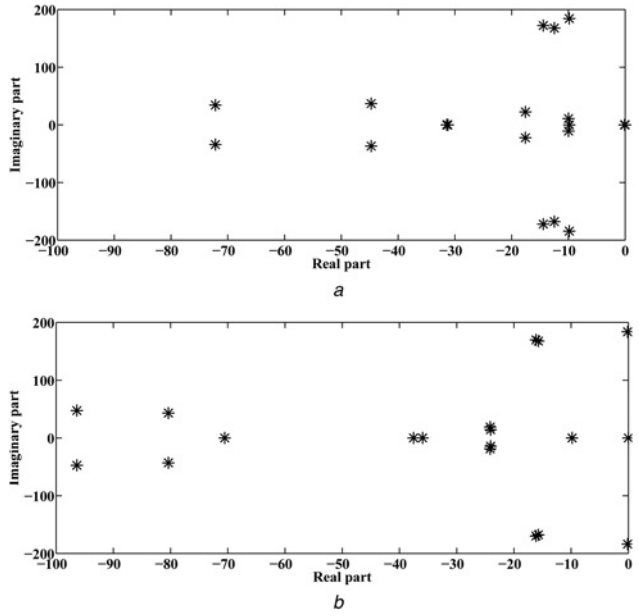

Fig. 5 *Eigenvalues near imaginary axis for*
a Islanded operation
b Grid-connected operation

The time-domain simulations are carried out in the MATLAB Simulink environment. The original non-linear models are employed in the transient simulation. However, VSCs are represented by means of averaged models. To avoid the starting procedures for induction motor and VSR loads, the simulation is initiated at the idling period. The pick-up period is initiated at $t = 1$ s. Results of the transient simulation corresponding to the islanded and grid-connected operations are produced in Figs. 6 and 7, respectively. The rotor speed of the newly added induction motor is close to system frequency in the idling period. Subsequently, the load torque is applied in the pick-up, which causes the rotor speed to fall. The system frequency is almost maintained constant by appropriately adjusting the source reference power settings in the event of transition from idling to pick-up periods. In grid-connected operation, the power exchange between the utility grid and microgrid in the pick-up is observed to be 798 W. For both the grid-connected and islanded modes of operation, the system retains stability after the load transition. However, oscillations are more during the grid-connected operation because of the parallel operation of droop-controlled sources with the utility grid.

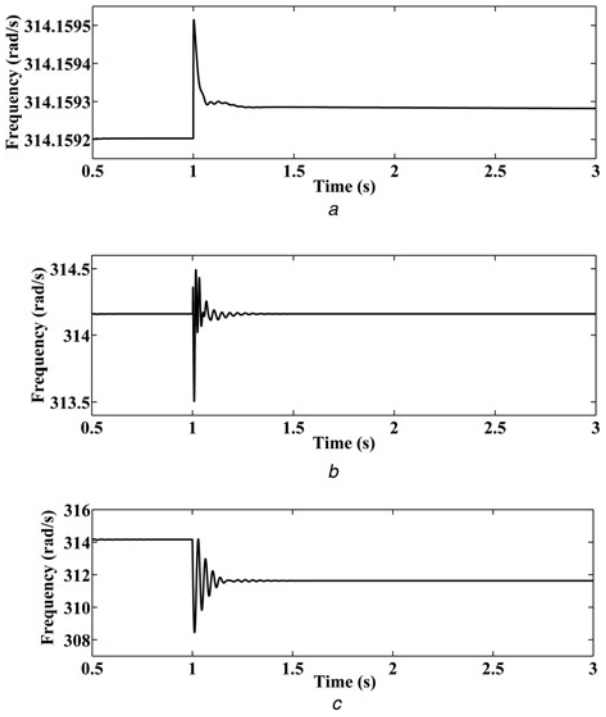

Fig. 6 *Dynamics of frequencies in islanded operation corresponding to*
a Global reference frame
b PLL of the newly added VSR fed DC load
c Rotor of the newly added induction motor

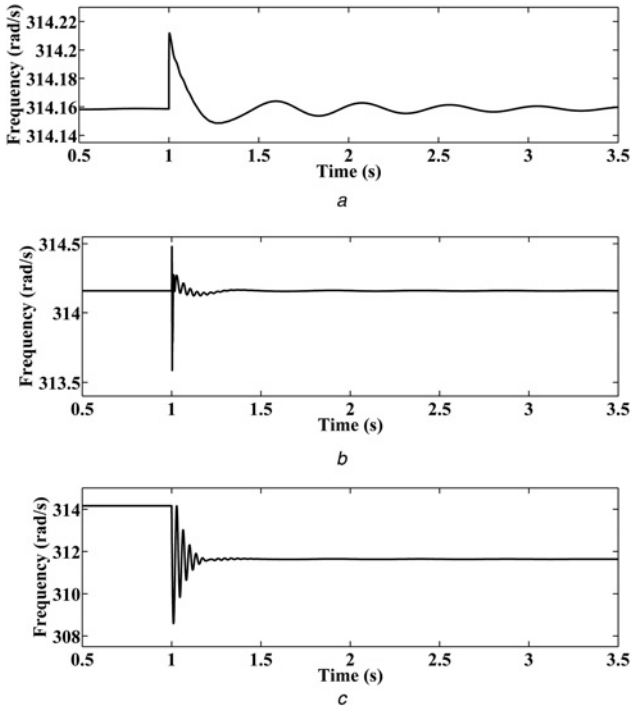

Fig. 7 *Dynamics of frequencies in grid-connected operation corresponding to*
a Global reference frame
b PLL of the newly added VSR fed DC load
c Rotor of the newly added induction motor

6 Conclusion

In this paper, a systematic procedure is prescribed for the small-signal stability analysis of a microgrid with the scope for general applications. By recognising that there can be many different types of loads in a microgrid, a unified modelling is carried out to represent the load dynamics. The representation of load dynamics is made in the form of two simple templates. It is shown that the dynamics of any load can be described through either of those two templates. The load templates are defined based on the state or non-state nature of the load current. In the same way, the dynamics of all the different types of sources are described through a single template. The organisation of the small-signal model of an element is explained based on those templates. After organising the small-signal load and source models in the prescribed formats, some common steps are to be followed, irrespective of the actual microgrid configuration, for the construction of the system state matrix. The steps involved in the construction of the system state matrix are explained in details. The application of the proposed generalised state-space modelling framework is made for investigating the stability of a microgrid with the simultaneous presence of R, RL, thermostatic, induction motor and VSR

J Eng 2016
doi: 10.1049/joe.2016.0045

loads. Finally, it is revealed from the case study that a stable system operation in the presence of both induction motor and VSR loads is possible with appropriate tuning of controller parameters.

7 References

[1] Lasseter R.H.: 'MicroGrids'. Proc. IEEE Power Engineering Society Winter Meeting, 2002, pp. 305–308

[2] Chandorkar M.C., Divan D.M., Adapa R.: 'Control of parallel connected inverters in standalone AC supply systems', *IEEE Trans. Ind. Appl.*, 1993, **29**, (1), pp. 136–143

[3] Coelho E.A.A., Cortizo P.C., Garcia P.F.D.: 'Small-signal stability for parallel-connected inverters in stand-alone AC supply systems', *IEEE Trans. Ind. Appl.*, 2002, **38**, (2), pp. 533–542

[4] Pogaku N., Prodanovic M., Green T.C.: 'Modeling, analysis and testing of autonomous operation of an inverter-based microgrid', *IEEE Trans. Power Electron.*, 2007, **22**, (2), pp. 613–625

[5] Liang H., Choi B.J., Zhuang W., *ET AL.*: 'Stability enhancement of decentralized inverter control through wireless communications in microgrids', *IEEE Trans. Smart Grid*, 2013, **4**, (1), pp. 321–331

[6] Kundur P.: 'Power system stability and control' (McGraw-Hill, New Delhi, India, 1994)

[7] Iyer S.V., Belur M.N., Chandorkar M.C.: 'A generalized computational method to determine stability of a multi-inverter microgrid', *IEEE Trans. Power Electron.*, 2010, **25**, (9), pp. 2420–2432

[8] Yazdanian M., Mehrizi-Sani A.: 'Distributed control techniques in microgrids', *IEEE Trans. Smart Grid*, 2014, **5**, (6), pp. 2901–2909

[9] Hassan M.A., Abido M.A.: 'Optimal design of microgrids in autonomous and grid-connected modes using particle swarm optimization', *IEEE Trans. Power Electron.*, 2011, **26**, (3), pp. 755–769

[10] Papadopoulos P.N., Papadopoulos T.A., Crolla P., *ET AL.*: 'Measurement-based analysis of the dynamic performance of microgrids using system identification techniques', *IET Gener. Transm. Distrib.*, 2015, **9**, (1), pp. 90–103

[11] Kahrobaeian A., Mohamed Y.A.-R.I.: 'Analysis and mitigation of low-frequency instabilities in autonomous medium-voltage converter-based microgrids with dynamic loads', *IEEE Trans. Ind. Electron.*, 2014, **61**, (4), pp. 1643–1658

[12] Alaboudy A.H.K., Zeineldin H.H., Kirtley J.: 'Simple control strategy for inverter-based distributed generator to enhance microgrid stability in the presence of induction motor loads', *IET Gener. Transm. Distrib.*, 2013, **7**, (10), pp. 1155–1162

[13] Diaz G., Moran C.G., Aleixandre J.G., *ET AL.*: 'Composite loads in stand-alone inverter-based microgrids – modeling procedure and effects on load margin', *IEEE Trans. Power Syst.*, 2010, **25**, (2), pp. 894–905

[14] Wang W., Zeng X., Tang X., *ET AL.*: 'Analysis of microgrid inverter droop controller with virtual output impedance under non-linear load condition', *IET Power Electron.*, 2014, **7**, (6), pp. 1547–1556

[15] Bottrell N., Prodanovic M., Green T.C.: 'Dynamic stability of a microgrid with an active load', *IEEE Trans. Power Electron.*, 2013, **28**, (11), pp. 5107–5119

[16] Radwan A.A.A., Mohamed Y.A.-R.I.: 'Analysis and active-impedance-based stabilization of voltage-source-rectifier loads in grid-connected and isolated microgrid applications', *IEEE Trans. Sustain. Energy*, 2013, **4**, (3), pp. 563–576

[17] Zhong Q.C., Nguyen P.L., Ma Z., *ET AL.*: 'Self-synchronized synchronverters: inverters without a dedicated synchronization unit', *IEEE Trans. Power Electron.*, 2014, **29**, (2), pp. 617–630

[18] Dong D., Wen B., Boroyevich D., *ET AL.*: 'Analysis of phase-locked loop low-frequency stability in three-phase grid-connected power converters considering impedance interactions', *IEEE Trans. Ind. Electron.*, 2015, **62**, (1), pp. 310–321

[19] Radwan A.A.A., Mohamed Y.A.-R.I.: 'Modeling, analysis, and stabilization of converter-fed AC microgrids with high penetration of converter-interfaced loads', *IEEE Trans. Smart Grid*, 2012, **3**, (3), pp. 1213–1225

[20] Yazdani A., Iravani R.: 'Voltage-sourced converters in power systems' (IEEE/Wiley, Piscataway, NJ, USA, 2010)